Received 9 July 2023; revised 17 September 2023; accepted 9 October 2023. Date of publication 11 October 2023; date of current version 26 October 2023.

Digital Object Identifier 10.1109/OJAP.2023.3323812

Synthesis of Plane-Wave Generator in 3-D Sphere Quiet Zone for Advanced Antenna Measurement by Hybridizing LSM and GA

HAIDONG CHEN [1,2] (Senior Member, IEEE), WEIJUN ZHONG [1], MU TAN [1], ZHAOLING HE [1], TING LI [1], QUAN XUE [1,2] (Fellow, IEEE), AND WENQUAN CHE [1,2] (Fellow, IEEE)

[1]School of Electronic and Information Engineering, South China University of Technology, Guangzhou 510641, China

[2]Guangdong Provincial Key Laboratory of Millimeter-Wave and Terahertz, South China University of Technology, Guangzhou 510641, China

CORRESPONDING AUTHOR: H. CHEN (e-mail: chenhd@scut.edu.cn)

This work was supported in part by the Guangdong Innovative and Entrepreneurial Research Team Program under Grant 2017ZT07X032, and in part by the National Natural Science Foundation of China under Grant 62271207.

ABSTRACT In this paper, we hybridize the Least Square Method (LSM) and Genetic Algorithm (GA) to efficiently synthesize the linear and planar array Plane Wave Generator (PWG) to create a 3-D Quiet Zone (QZ) with high performance for the antenna pattern measurement in a chamber with limited space. Based on the PWG with an 8-element linear array, the amplitude and phase deviations of 0.89 dB and 14.50° are obtained in a circular QZ with a diameter of 7λ, and that with an 8 × 8-element plane array achieves 1.09 dB and 14.89° deviations in a 3-D sphere QZ. The synthesized results using other existing algorithms based on different configurations of PWG are compared and the synthesis errors are discussed. Simulation results show the robustness and high efficiency of the proposed algorithm on 2-D and 3-D PWG synthesis.

INDEX TERMS Plane-wave generator, least squares, genetic algorithm, hybridization, 3D quiet zone, antenna measurement.

I. INTRODUCTION

AT PRESENT, the research on 5G communication technology and the production of relevant prototypes have set off a wave of innovation in the industry all over the world [1]. As one of the key technologies of 5G communication, the large-scale antenna array has attracted extensive attention in the industry [2], which generally has hundreds or even thousands of antenna elements with very large apertures [3]. This characteristic brings difficulty both from the antenna design and measurement sides. Radiation pattern measurement is one key process in the qualification of any antenna and the measurement method is mainly classified into some different methods: far-field (FF), near-field (NF), and compact antenna test range (CATR).

The FF method requires the antenna under test (AUT) to be illuminated by a uniform plane wave. To achieve this uniform planar wave irradiation, the simplest method is to place the AUT in the far-field region of a source [4], which is also named as Fraunhofer zone and can be defined as the distance where is bigger than r calculated as [5]

$$r \geq \frac{2D^2}{\lambda} \tag{1}$$

where D is the diameter of the smallest sphere that contains the AUT, and λ is the wavelength of the AUT.

The FF method has the advantage of recording the magnitude and phase of the electric field of AUT directly based on very simple mechanical positioners. However, this method may need a hundred meters to achieve the far-field condition calculated as equation (1) if the AUT has a large aperture at a high-frequency band. This situation brings the high cost of an anechoic chamber for indoor measurement of significant uncertainties for outdoor measurement. The NF method is to scan the AUT in both magnitude and phase on

a two-dimensional surface and then mathematically transform these results into the far-field pattern [6], [7], [8]. A compact low-cost anechoic chamber could be used to set up the corresponding equipment to offer mechanical surface scanning of planar, cylindrical, and spherical [9]. However, this method requires many discrete magnitude and phase data with high accuracy acquired by the mechanical scanner or positioner, which significantly reduces the measurement efficiency due to time consumption. The CATR method uses a source antenna and one or more reflectors to shine on an AUT in the Quiet Zone (QZ) in which the amplitude and phase deviations are restricted and the field behaves like a plane wave. The CATR method begins to be widely used as the distance between the QZ and reflectors is much smaller than that of the traditional FF method [10]. However, to achieve the desired performance over a wide frequency range, the CATR method has a very high-cost reflector whose measurement of upper frequency and accuracy links to the reflector's shape, surface roughness, and errors.

Another effective method is to use a plane wave generator (PWG) consisting of some source elements with specified locations and their weights of amplitude and phase [11], [12], and has been adopted in the latest 3GPP standards as a test method for 5G mm-Wave antenna measurement [13]. The advantages of the PWG method are competitive size, appropriate cost, and the ability to directly measure the antennas by using the FF method efficiently [14], which attracts much interest in academia and industry. However, unlike the FF method, those weights of amplitude and phase of source elements need to be synthesized and pre-determined efficiently to achieve the desired plane wave in the QZ. In the 1970s, Bucci et al. carried out plane wave synthesis for real-time imaging by using a radar array through an iterative algorithm [14], and Hill synthesized the plane wave with a combination of line source and ring, based on the Fourier series method and the least square method (LSM) in 1985 [15]. In 2019, Sun et al. used a genetic algorithm (GA) to synthesize the PWG for OTA testing in a small chamber, the distance between the PWG and the QZ was 20λ (1.71 m) at 3.5 GHz in which the deviation of amplitude and phase were 1dB and 10 degrees, respectively [16]. In 2020, Catteau et al. used a simple linear taper method and a truncated raised cosine taper method for amplitude control to the edges of the source array, which helped to realize the deviation of amplitude and phase of ±0.75 dB and ±7.5 degree in QZ, respectively, at the frequency of 28 GHz [4]; Peng et al. compared three algorithms of LSM, singular value decomposition (SVD), and sparse optimization algorithms in the synthesis processes, with less difference, was found among these different algorithms as the amplitude and phase deviations are approximate ±1 dB and ±2 degree, respectively [17]. In 2021, Krasov et al. implemented the linearly constrained minimum variance (LCMV) beamforming algorithm to generate a plane wave shining on the QZ from the desired direction, and the deviation of amplitude and phase were 0.87 dB and 7.55 degrees [18], respectively.

Synthesis of complex coefficient excitation using different algorithms has made some ideal progress; however, each existing method has its limitations. The traditional regression method like the LSM algorithm suffers from the problem of an ill-conditioned transfer matrix which causes large errors from small disturbances. This problem may be solved by reducing data relevance through many sampling data; however, this method impacts the efficiency of the synthesis process and may not solve the issue fundamentally. The global optimization algorithm such as GA can be used to determine the amplitude and phase weights of source elements efficiently; however, the adoption of the brute force approach typically leads to heavy computational overhead as well. Thus, a hybrid approach to the PWG synthesis has been applied which hybridizes GA for the search for the optimal feed position and quadratic programming to achieve the optimal excitations [19]. This approach is also adopted in [20], which has a relative error below -30 dB of the plane wave in the AUT rectangular area.

Moreover, most syntheses of PWG only focus on the amplitude and phase deviations on the line or 2D plane paralleling the PWG at the center position of QZ. Some researchers have considered the 3D cylindrical QZ [21], [22], [23] and even evaluated the 3D cuboidal region with an extension of 30 cm in the QZ facing the PWG [4]. However, to the authors' knowledge, only the work in [23] inspects the QZ field at a different position along the propagation direction, and all the existing arts have not performed the synthesis based on those discrete points from the entire 3D region, which is very important during the measurement on those 5G devices [2].

In this paper, we propose a hybrid algorithm based on LSM and GA to obtain a spherical QZ with uniform electric field amplitudes in the full 3D region and a consistent phase in each phase plane facing the PWG. The initial solution is obtained with LSM by solving the transmission matrix in space between the AUT and the PWG, and the final optimal solution is achieved using GA by changing the correlation coefficient. This hybrid method obtains the optimal solution efficiently, based on its globality to avoid getting into local optimization before getting a solution that meets the expected criteria. The paper is organized as follows: Section II briefly describes the system measurement model and the synthesis model and Section III presents the basic concepts of LSM and GA and the proposed concept of hybridizing LSM and GA for PWG synthesis. The numerical approach, process, and key factors for the PWG synthesis based on the ideal antenna array are demonstrated in Section IV, and the results with different types of sources and targets are presented in Section V. The performance comparisons to existing arts and the synthesis errors are discussed in Section VI and the conclusions are summarized in Section VII.

II. MEASUREMENT SYSTEM AND SYNTHESIS

Figure 1 shows the whole model of the measurement system based on the PWG which consists of PWG, 2D positioner,

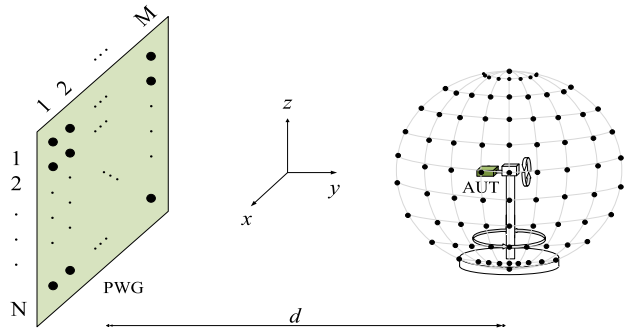

FIGURE 1. Model of the measurement system based on the PWG.

and AUT. The PWG in practice can be divided into three main blocks: the feeding network with power dividers or combiners, beam-forming networks with phase shifters and attenuators, and the various antennas or probes as the source elements. The 2D positioner is commonly used in the great circle test method [24], which fixes the AUT and rotates in both the azimuth and the roll direction to achieve a 3D antenna pattern. The AUT should be within the 3D region of QZ of which performances are determined by the characteristic of the PWG and distance d between the AUT and PWG. The amplitude and phase deviations in QZ determine the measured accuracy of AUT, which have been defined as 1 dB and 22.5° as the common criterion for the measurement of most antenna types [25]; however, they are expected to be as small as possible.

The actual synthesis process of PWG is to optimize the complex amplitude weights of discrete source elements to create approximate plane waves with certain limited deviations in QZ under the condition of given d shown in Figure 1 much smaller than the r calculated from equation (1).

It is well known that the field strength P of arbitrary point E radiated by a point source in any finite radial distance can be simplified as

$$P = \hat{A}\frac{e^{-j\frac{2\pi}{\lambda}r}}{r} \tag{2}$$

where $\hat{A}$ is the monopole amplitude, λ is the wavelength, and r is the distance between the source and field points, respectively [26]. According to the measurement system shown in Figure 1, if we consider the PWG consists of an array with $K(M\times N)$ ideal source elements and each generated wave by the element has the same polarization as that of the AUT, then any field strength of discrete point away from PWG is the superposition of the radiation of each element which is simplified as [17]:

$$P_l = \sum_{k=1}^{M\times N} w_k \frac{e^{-j\frac{2\pi}{\lambda}r_{\mathrm{kl}}}}{r_{\mathrm{kl}}} \tag{3}$$

where w represents the complex weight value of the source element and r_{kl} is the distance from the k-th source element to the l-th sampled point. The goal of the PWG synthesis in this work is to determine the optimal excitation w_k of each source element to generate desired field distributions based on combinations of each field strength on a specified 2D plane or in a full 3D region.

III. SYNTHESIS METHOD

A. LSM SOLUTION

Based on the definition of QZ, the deviations of amplitude in the full 3D region and those of phase on a specified 2D plane facing PWG are required to be as small as possible. If we assume that the count of the 2D/3D sampling point in QZ is L, then we have

$$P = \mathrm{HW} \tag{4}$$

where $P = [P_1, P_2, \ldots, P_{\mathrm{L}}]^T$, $\mathrm{W} = [w_1, w_2, \ldots, w_{\mathrm{K}}]^T$, and H is an $L\times K$ matrix given by

$$H = \begin{bmatrix} \frac{e^{-jkR_{11}}}{R_{11}} & \cdots & \frac{e^{-jkR_{1K}}}{R_{1K}} \\ \vdots & \ddots & \vdots \\ \frac{e^{-jkR_{L1}}}{R_{L1}} & \cdots & \frac{e^{-jkR_{\mathrm{LK}}}}{R_{\mathrm{LK}}} \end{bmatrix} \tag{5}$$

If the derivations of field distribution in the specified region, the element position, and the number of elements have been given, then based on equations (4)–(5) and the principle of LSM [27], we can obtain the complex weight W as

$$W = \left[H^T \cdot H\right]^{-1} H^T P \tag{6}$$

LSM has the advantage of finding an approximate field synthesis solution to determine the excitation of source elements efficiently; however, the disadvantage is that the coupling matrix and the right-hand side vector are disturbed by unavoidable numerical errors, which may cause significant errors during the numerical process [17].

B. GA SOLUTION

GA is a global optimization algorithm that provides robust searches in a complex space to find the optimal solution quickly [28]. The basic process of GA is to generate the random population, encode the initial population, evaluate the fitness for the selection of a new population, and the mutation to obtain a new generation of sample groups, as shown in Table 1.

With the initial random population, GA can speculate on new searches with an expected improved performance efficiently by exploiting historical information contained in the gene pool based on many points and random transition rules. This is the reason that GA attracts much interest in research and industrial communities, and is widely used to solve complex problems in different fields. However, when GA is directly used to optimize the excitation coefficient of PWG in this work, long iteration time and failure of finding the optimal solution may occur due to the weak mountain climbing ability and falling into local optimization [29].

TABLE 1. Basic flow of genetic algorithm.

Algorithm:	GA
Start: Generate random population of n chromosomes (suitable solutions for the problem)	
Coding: Select a suitable coding method for the initial population and carry out the coding	
Fitness: Evaluate the fitness f(x) of each chromosome x in the population	
New population: Create a new population by repeating following steps until the new population is complete	
Selection: Select two parent chromosomes from a population according to their fitness (the better fitness, the bigger chance to be selected)	
Crossover: With a crossover probability cross over the parents to form a new offspring (children). If no crossover was performed, offspring is an exact copy of parents.	
Mutation: With a mutation probability mutate new offspring at each locus (position in chromosome).	
Accepting: Place new offspring in a new population	
Replace: Use new generated population for a further run of algorithm	
Test: If the end condition is satisfied, stop, and return the best solution in current population	
Loop: Go to fitness calculation	

C. HYBRID ALGORITHM

Now we know that a relatively good solution may be obtained directly by LSM if the array matrix is not ill-conditioned with a potential risk to calculation stability, and the algorithm iteration can be accelerated with an optimal solution if an appropriate initial value is given by using GA. According to this consideration and the fact that GA can be easily compatible with other algorithms, the appropriate optimal results are possible to be obtained efficiently by hybridizing LSM and GA. In this work, the LSM is used to obtain the initial solution of the complex weight matrix of W in (6) at first, and the GA is used to obtain the final optimal solution at last without the limitation of restrictive assumptions on the search space. The basic implementation progress of the proposed hybrid algorithm is shown in Figure 2.

Figure 2 also shows the detailed process of GA in which the coding of initial amplitude and phase is the key process at the start of GA that determines the efficiency of genetic evolution, as it directly affects the operation of genetic operators such as crossover and mutation. For example, the rates of crossover and mutation operation can be improved from the reduction of computational complexity when using specific coding such as real-coding, which is convenient for genetic search in a large space, and the mixed-use of optimization methods, as the length of real-coding, is equal to the number of decision variables.

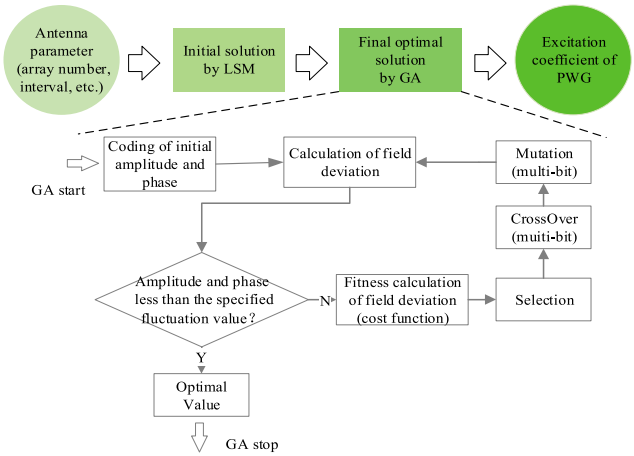

FIGURE 2. Basic PWG synthesis using the hybrid algorithm with LSM and GA.

IV. NUMERICAL METHOD AND PROCESS

A. PWG DESIGN

The approach of the proposed hybrid algorithm is to provide good estimates of the design parameters as guidelines and to assess the achievable performances before adjusting the parameters of physical components in practice. Based on the proposed algorithm, it is possible to obtain the deviations close to the absolute minimum; however, this identification of the absolute minimum requires a very large number of iterations and computation time due to the high non-linearity of the problem. Thus, any extensive investigation on the convergence of the algorithm needs to be carried out with the trade-off between accuracy and time consumption.

In this work, the PWGs with both linear array and planar array are investigated, the linear array has 8 source elements and the planar one has 8×8 source elements, of which the element spacing is 2.85λ at the frequency of 3.5 GHz while the distance d between PWG and AUT in Figure 1 is 2 m. The QZ is a 3D sphere with an expected radius of 0.3 m. The goal is to synthesize the amplitude and phase of each source element in both linear array and planar array to achieve the optimal deviations along X-direction (1-D), on XOY or XOZ plane (2D) or in the full spherical region (3D) of QZ, respectively. The initial excitation which affects the optimization efficiency and the robustness of the program is obtained based on equations (1)–(6) by using LSM at first and then taken as the initial input parameters of GA for further optimization.

B. COST FUNCTION AND TARGETS

According to the plane wave synthesis method based on the hybrid algorithm with LSM and GA shown in Figure 2, the deviations of amplitude and phase in QZ can be taken as the optimization goal and the cost function is constructed as:

$$h = h_1/a + h_2/b \tag{7}$$

where $h_1 = |\max\{amplitude\} - \min\{amplitude\}|$ and $h_2 = |\max\{phase\} - \min\{phase\}|$ are the amplitude and phase deviations acquired from the X-axis, XOY or XOZ plane, or whole

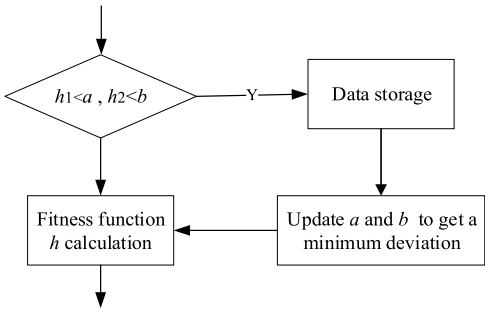

FIGURE 3. Minimum deviation obtainment from the basic process.

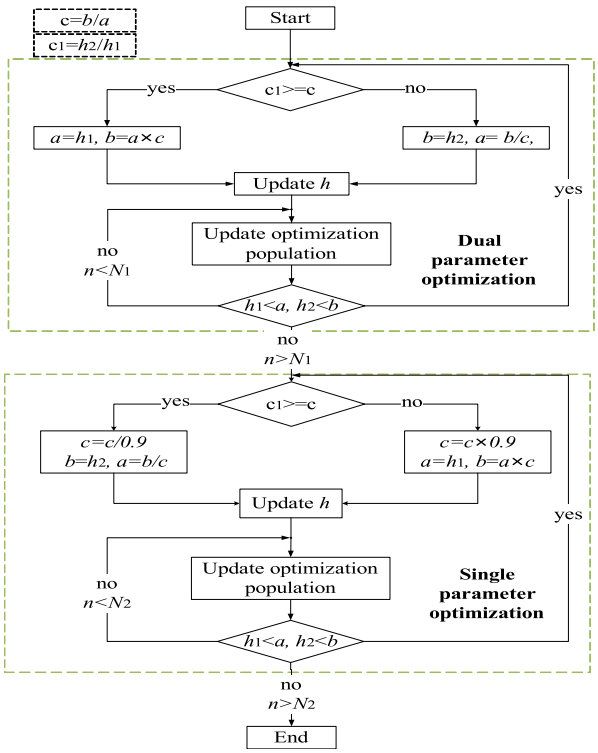

FIGURE 4. Process of minimum deviation search in detail.

sphere in the QZ, respectively; a and b are the weights of amplitude and phase which are related to the performance requirements of QZ, for example, if we set $a = 2$ and $b = 20$, then the GA process will stop once the general deviations of amplitude and phase are within 2 dB and 20°.

C. MINIMUM DEVIATION SEARCH

The amplitude and phase deviations of h_1 and h_2 are expected to be as small as possible. Figure 3 shows our proposed process of the minimum value search of h_1 and h_2, by rerunning the optimization process based on downscaled a and b, and Figure 4 shows the entire process in detail. The whole process is divided into two steps which are named Dual Parameter Optimization (DPO) and Single Parameter Optimization (SPO). DPO is to get smaller deviations of amplitude and phase deviations by scaling down a (and b) and keeping c unchanged. For example, the GA process

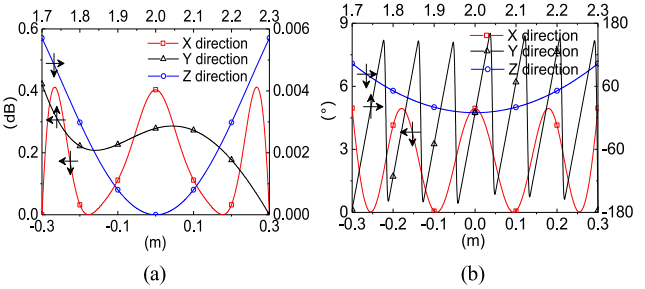

FIGURE 5. The deviations of (a) amplitude and (b) phase along the X/Y/Z-axis of 1-D optimization target based on linear array.

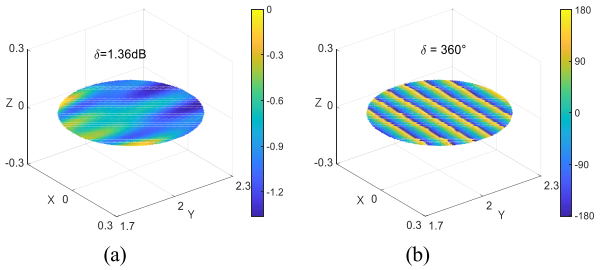

FIGURE 6. Optimized amplitude (a) and phase (b) distributions of 1-D optimization target on XOY plane based on linear array with maximum deviations δ.

may stop with the deviations of 1.5 dB and 18° if we set $a = 2$ and b=20, then a and b are updated to 1.5 and 15, as c_1 equals 12 which is bigger than c of 10. This helps to reduce the deviations with the defined ratio at the same time. SPO is to get smaller deviations by scaling down a (or b) only when the number of iterations n of the proposed DPO reaches the maximum value N_1 and to stop when it reaches the maximum value N_2. Both N_1 and N_2 are selected depending on the computation resources, synthesis efficacy, and the observation of fitness reduction.

V. NUMERICAL RESULTS

A. LINEAR ARRAY

When an 8-elements linear array is set symmetrically along the X-axis as shown in Fig. 1. The amplitude and phase distributions along the X-axis in QZ based on this linear array are axisymmetric as well, and those along the Y-axis and Z-axis are equivalent to be generated by a point source.

Figures 5 and 6 show the synthesized deviations of the amplitude and phase along the $X/Y/Z$-axis using the 1-D optimization target based on the 8-element linear array, and the 2-D sectional view on XOY, respectively. Figure 7 shows the error bars of those distributions parallel to the X-axis sampled from the XOY plane shown in Fig. 6(b), from which we can see that the deviations located at 2 m (QZ center) are only 0.41 dB and 4.96°; however, those in whole regions are approximate 1.36 dB and 17.41°, respectively.

Figures 8 and 9 show the optimized results of the amplitude and phase along the $X/Y/Z$-axis using the 2-D optimization target based on the same 8-element linear array, and the 3-D full view and 2-D sectional view of the results,

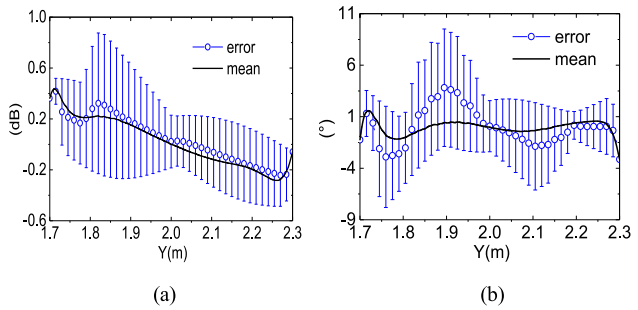

FIGURE 7. The error bars of (a) amplitude and (b) phase distributions parallel to the X-axis sampled from the XOY plane of 1-D optimization target on the linear array.

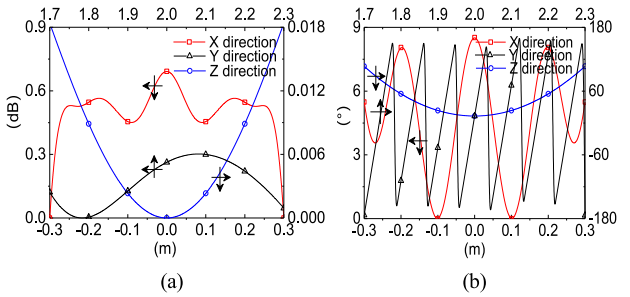

FIGURE 8. The deviations of (a) amplitude and (b) phase along the X/Y/Z-axis of 2-D optimization target based on the linear array.

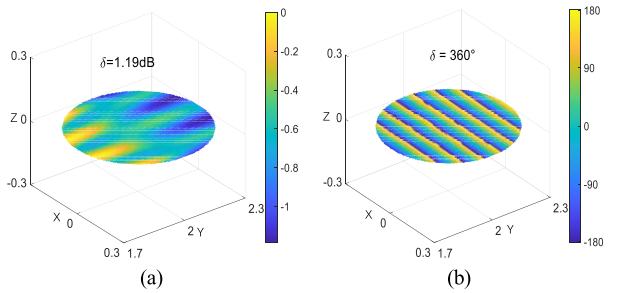

FIGURE 9. Optimized amplitude (a) and phase (b) distributions of 2-D optimization target on XOY plane based on linear array with maximum deviations δ.

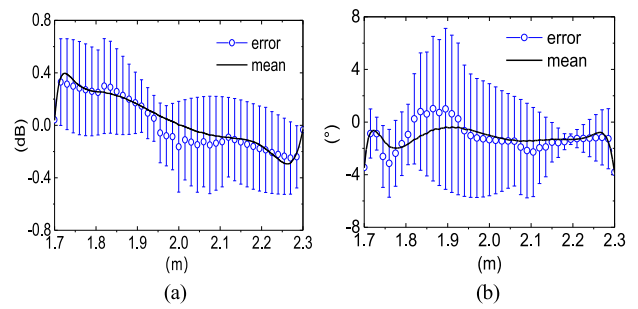

FIGURE 10. The error bars of (A) amplitude and (B) phase distributions parallel to the X-axis sampled from the XOY plane of 2-D optimization target on a linear array.

respectively. Figure 10 shows the error bars of those distributions parallel to the *Y*-axis sampled from the *XOY* plane shown in Fig. 9(d), from which we can see that the deviations located at the QZ center deteriorated from 0.41 dB to 0.69 dB and from 4.96° to 8.52°; however, those in whole

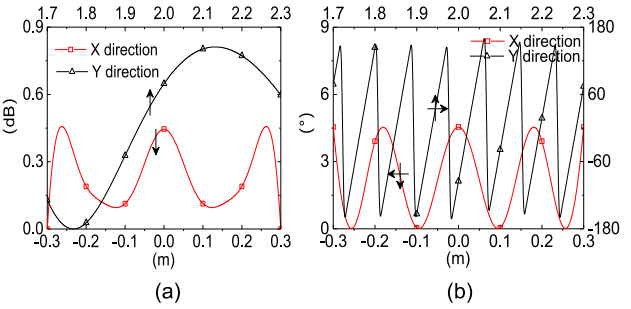

FIGURE 11. The deviations of (a) amplitude and (b) phase along the X/Y/Z-axis of the 1-D optimization target based on the planar array.

regions are improved to from 1.36 dB to 1.19 dB and from 17.41 to 13.08°, respectively. According to the optimized results of the linear array shown in Figure 5-10, we can know that: 1) the field deviations along the *X*-axis based on the 1-D optimization target are smaller than those based on the 2-D optimization target; 2) the field deviations based on the 1-D target on the *XOY* plane and in QZ are more uneven than those based on 2-D target; 3) the amplitude and phase distributions along the *Z*-axis cannot be optimized due to the characteristic of the linear array.

B. PLANAR ARRAY

The planar array is more suitable to generate the plane wave based on the same principle of a linear array. In this work, a planar array with 8×8 elements is used for the demonstration of our proposed 3D optimization with the hybrid algorithm. Different optimization targets based on those amplitude distributions from the *X*-axis, *XOZ* plane, and the whole sphere are applied, along with the targets based on the normalized phase distributions by removing the inherent phase shift. Meanwhile, the number of unknowns to be dealt with in the global algorithm can be down to a quarter, which simplifies the field calculation and increases the convergence speed, as the excitation of the planar array usually is both symmetric about the *X*-axis and *Z*-axis and the field distributions in QZ exhibit the same property. Figure 11-13 and Figure 14-16 are the optimized results of the 8×8-element planar array based on the optimization target of the field distributions acquired from the *X*-axis and the *XOZ* plane. Figures 17-19 are the results based on the whole sphere optimization target.

Table 2 lists the optimal results based on the planar array and different optimization targets shown in Figure 11-16, along with the results based on the linear array shown in Figure 5-10 for comparison. It is obvious that the amplitude and phase deviations along the *X*-axis are only 0.45 dB and 4.52° if the 1-D target is selected, as the field distribution along the *X*-axis is considered only during the optimization; however, those on the 2-D plane are 1.21 dB and 19.61°, and those in the 3-D sphere are 1.59 dB and 20.00°; 2) compared to those results based on 1-D optimization target, the deviations on *XOZ* plane are improved to 0.62 dB and 7.72° when 2-D optimization target is applied, also those deviations in

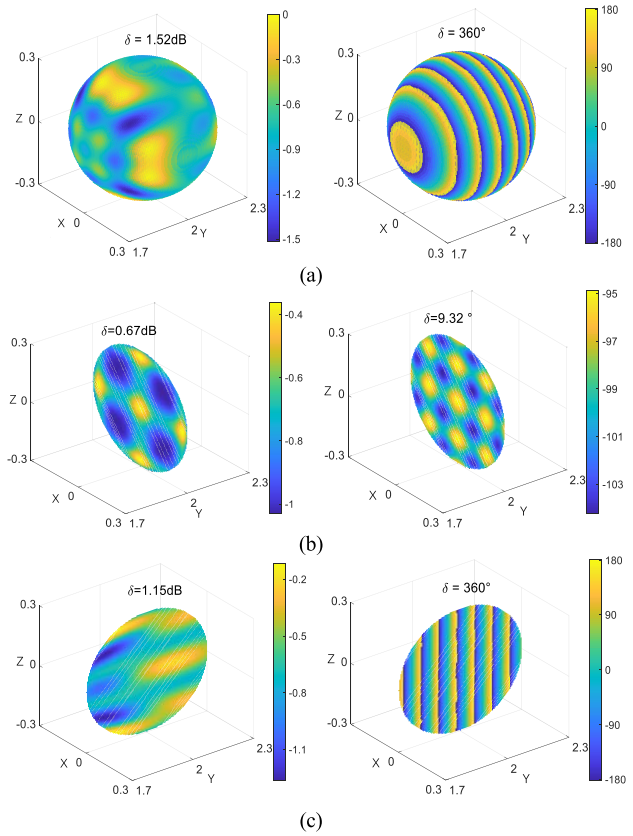

FIGURE 12. Optimized amplitude (left) and phase (right) distributions of 1-D optimization target based on the planar array with maximum deviations δ. (a) 3-D full view, (b) 2-D XOZ sectional view, (b) 2-D YOZ sectional view. 2-D XOY sectional view is the same as (b).

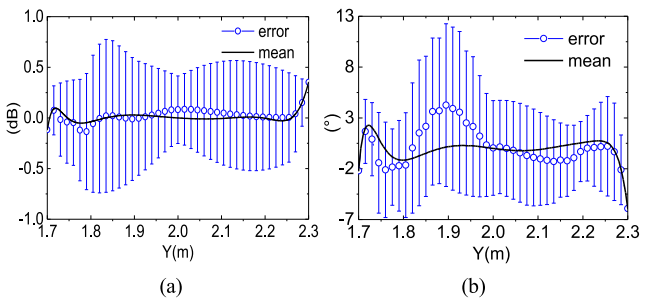

FIGURE 13. The error bars of (a) amplitude and (b) phase on the section parallel to the XOZ plane sampled from the whole sphere of 1-D optimization target based on the planar array.

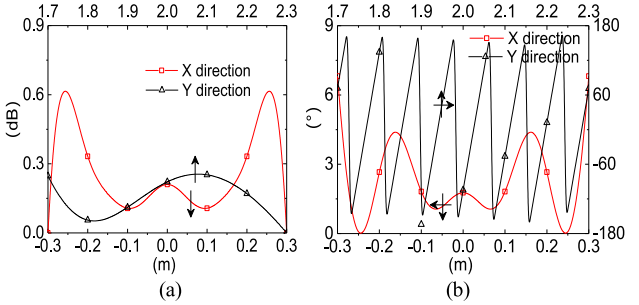

FIGURE 14. The deviations of (a) amplitude and (b) phase along the X/Y/Z-axis of the 2-D optimization target based on the planar array.

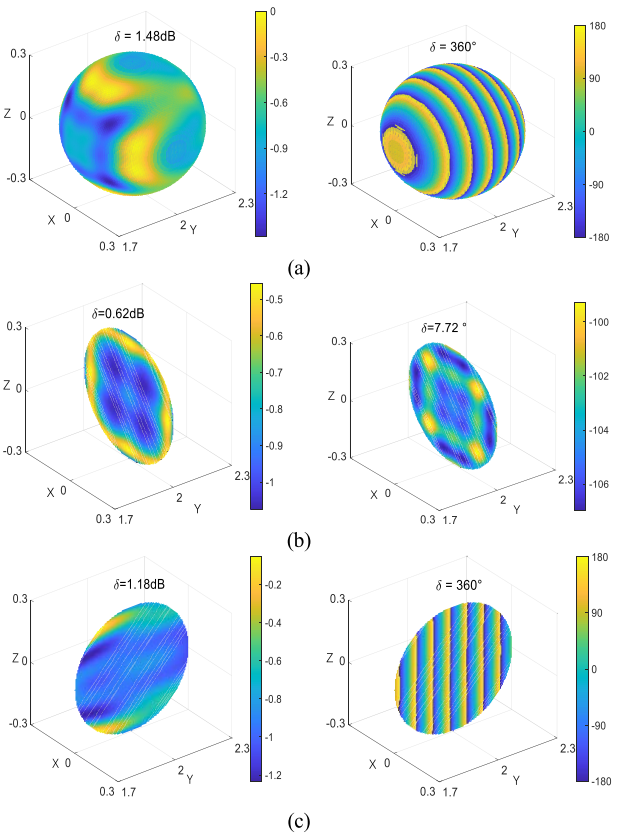

FIGURE 15. Optimized amplitude (left) and phase (right) distributions of 2-D optimization target based on the planar array with maximum deviations δ. (a) 3-D full view, (b) 2-D XOZ sectional view, (c) 2-D YOZ sectional view. 2-D XOY sectional view is the same as (c).

the sphere QZ are improved to 1.48 dB and 18.01°; however, those along the *X*-axis predictably deteriorate to 0.62 dB and 6.82°; 3) the amplitude and phase deviations along the *X*-axis and on the plane, e.g., *XOY* (*YOZ*) and *XOZ*, are deteriorated based on 3-D optimization target; however, those deviations in the whole sphere are improved significantly to 1.09 dB and 14.89° which are acceptable in practice.

VI. DISCUSSION

A. RESULTS COMPARISON

According to the simulated results, the qualities of a plane wave in the whole QZ generated by the proposed comprehensive optimization using the hybrid algorithm are improved significantly based on the 3-D optimization target. Different optimization results may be obtained by using different cost functions composed of different amplitude and phase coefficients a and b in (7), which helps to get desired field distributions with specified deviations of the field.

Table 3 lists the compared results based on different optimization targets using different algorithms [30], [31], [32], from which we can see that: 1) most existing arts take the 2-D square planes as the optimization targets only and the performances in the whole 3-D QZ are

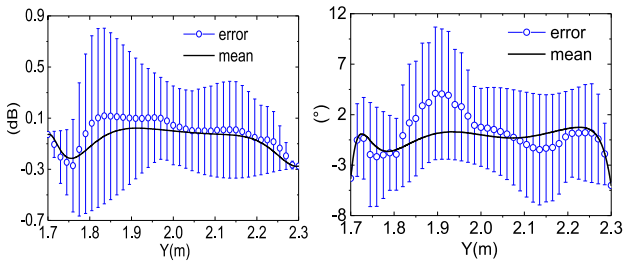

FIGURE 16. The error bars of (a) amplitude and (b) phase on the section parallel to the XOZ plane sampled from the whole sphere of 2-D optimization target based on planar array.

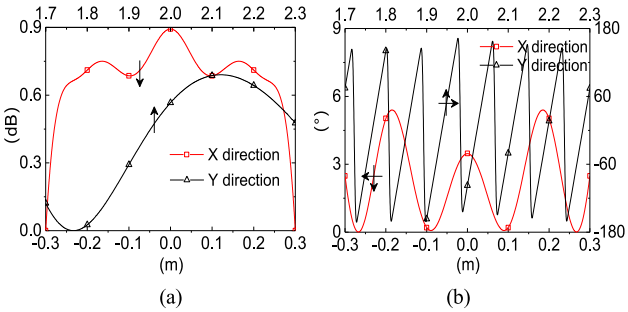

FIGURE 17. The deviations of (a) amplitude and (b) phase along the X/Y/Z-axis of 3-D optimization target based on planar array.

TABLE 2. Comparison of optimization results based on different antenna array forms and objectives.

Array Type	Linear Array		Planar Array			Position
Opt. Target	1-D	2-D	1-D	2-D	3-D	
Amp. Dev. (dB)	0.41	0.69	0.46	0.62	0.89	Along X-axis
	1.36	1.19	1.15	1.18	1.02	*XOY* plane
	0.42	0.71	0.67	0.62	0.89	*XOZ* plane
	0.42	0.3	1.15	1.18	1.02	*YOZ* plane
	1.36	1.19	1.52	1.48	1.09	3-D sphere
Phas. Dev. (°)	4.96	8.52	4.55	6.82	5.42	Along X-axis
	17.41	13.08	19.61	18.19	14.85	*XOY* plane
	98.63	102.11	9.32	7.72	11.01	*XOZ* plane
	-	-	19.61	18.19	14.85	*YOZ* plane
	-	-	20	18.01	14.89	3-D sphere

The phase deviations in the 3-D sphere are normalized by removing the inherent phase shift

ignored, this brings the significant risk of antenna measurement because the performance of QZ in 3-D region may be not acceptable, for example the amplitude and phase deviations are up to 43.10 dB and 360° in the sphere with the diameter of 20λ based on 21×21 source array with 20λ distance and; 2) compared to the optimized results based

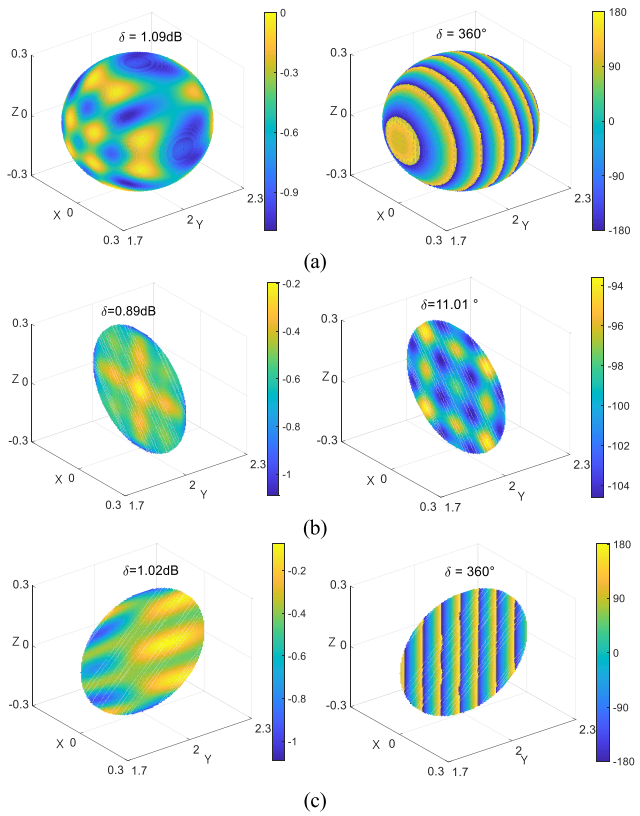

FIGURE 18. Optimized amplitude (left) and phase (right) distributions of 3-D optimization target based on planar array with maximum deviations δ. (a) 3-D full view, (b) 2-D XOZ sectional view, (c) 2-D YOZ sectional view. 2-D XOY sectional view is same as (c).

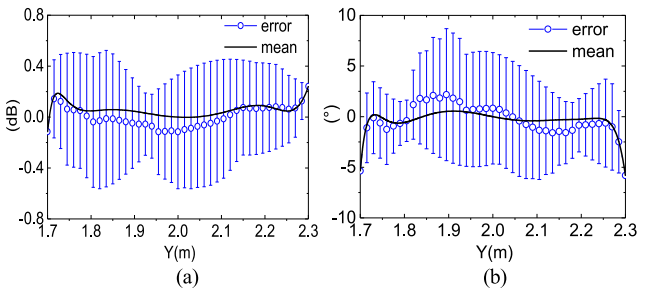

FIGURE 19. The error bars of (a) amplitude and (b) phase on the section parallel to the XOZ plane sampled from the whole sphere of 3-D optimization target based on planar array.

on the 2-D square planes, it is high efficiency using the 2-D circular planes at the optimization target, however, it also faces the same risk; 3) the optimization based on 3-D sphere region can guarantee the performance on the 1-D axis, 2-D circular planes, and 3-D sphere regions; 4) the hybrid algorithm of LMS and GA helps to achieve the smaller deviations of amplitude and phase; 5) the optimized diameters of the QZ in which the amplitude and phase deviations of 1.1 dB and 15° are 7λ, 11λ, 14λ,and 26λ based on the give sizes of source array of 8×8, 11×11, 21×21, 32×32 and the distance of 23λ, 20λ, 20λ, and 42λ.

Those optimized and compared results listed in Table 3 prove the advantage of our proposed hybrid algorithm;

TABLE 3. Comparison of the quiet zone quality obtained by other people's algorithms.

Ref.	Algorithms	PWG		Distance	QZ		Optimized Deviation Amplitude(dB)/ phase (°)		
		N_{elem}	Element Space		Optimization Target	Size	1-D (*X*-axis)	2-D (*XOZ*)	3-D
[4]	SLT, TRCT	32×32	1.05λ	42λ	Square Plane	$(28\lambda)^2$	×	1.50/15.00	×
[16]	GA	21×21	1λ	20λ		$(20\lambda)^2$	×	1.00/10.00	×
[17]	SVD	11×11	1.75λ	20λ		$(9.33\lambda)^2$	×	2.00/4.00	×
	LSM	21×21	1λ	20λ		$(18\lambda)^2$	×	0.15/0.47	×
	SVD						×	0.21/0.54	×
	SOA						×	0.21/0.51	×
[18]	LCMV	17×22	0.6λ	23.33λ		$(6.42\lambda)^2 \times 1.52\lambda$	×	1.00/10.00	0.87/7.55
[30]	LSM	21×21	1λ	32λ		$(20\lambda)^2$	×	1.00/7.00	×
[31]	LSM	9×14	0.75λ	8.67λ		$4.7\lambda \times 7.8\lambda$	×	1.11/8.50	×
	PSO						×	0.73/10.20	×
[32]	ABOMP	83	~1.7λ	24.5λ	Circular Plane	$(3.5\lambda)^2 \times \pi$	×	0. 89/7.70	×
This work	Hybrid Algorithm	11×11	1.75λ	20λ	Square Plane (*XOZ*)	$(9.33\lambda)^2$	0.05/0.31	0.13/0.62	9.11/42.18
		21×21	1λ	20λ		$(20\lambda)^2$	0.55/5.74	0.86/7.12	43.10/360
		21×21	1λ	20λ		$(18\lambda)^2$	0.06/0.63	0.07/0.97	24.20/360
		32×32	1.05λ	42λ		$(28\lambda)^2$	0.08/1.10	0.16/2.50	13.60/360
		21×21	1λ	32λ		$(20\lambda)^2$	0.007/0.05	0.15/1.62	60.08/360
		9×9	0.75λ	8.67λ		$(4.7\lambda)^2$	0.003/0.03	0.01/0.08	2.47/360
		14×14	0.75λ	8.67λ		$(7.8\lambda)^2$	0.01/0.19	0.04/0.62	32.06/360
		1×8	2.85λ	23λ	Circular Plane (*XOZ*)	$(7\lambda)^2 \times \pi/4$	0.41/4.96	1.19/13.08 (*XOY*)	×
		11×11	1.75λ	20λ		$(9.33\lambda)^2 \times \pi/6$	0.05/0.31	0.05/0.60	0.54/8.32
		21×21	1λ	25λ		$(18\lambda)^2$	0.001/0.01	0.001/0.02	1.60/24.75
		32×32	1.05λ	42λ		$(28\lambda)^2$	0.08/1.10	0.13/2.42	1.05/16.50
		8×8	2.85λ	23λ	Sphere	$(7\lambda)^3 \times \pi/6$	0.45/4.52	0.62/7.72	1.09/14.89
		11×11	1.75λ	20λ		$(11\lambda)^2 \times \pi/6$	0.45/5.81	0.50/7.38	0.76/12.78
		21×21	1λ	20λ		$(14\lambda)^3 \times \pi/6$	0.0003/0.005	0.0005/0.006	1.09/13.33
		32×32	1.05λ	42λ		$(26\lambda)^3 \times \pi/6$	0.003/0.024	0.004/0.047	0.82/11.97

however, these optimized results are based on the ideal source elements which may deteriorate when the actual antenna probes are loaded. This problem could be solved by using the calculated, simulated, or measured performances of the actual probes rather than those of the ideal elements, and the consideration of the mutual couplings converting into the mutual impedance during the QZ synthesis.

It should be note that there is no limitation on the element space of PWG as it is not required to scan the beam with the risk of grating lobe generation in traditional antenna array. Moreover, the distance between the PWG and QZ is expected to be as short as possible. We choose different parameters of PWG related to the performances of QZ, such as the count of element, the element space, and the distance from the PWG to QZ to verify our proposed hybrid algorithm and compare the results with other algorithms.

B. ERRORS

This proposed optimization algorithm on plane wave synthesis assumes that the source elements are with continued amplitude and phase values; however, most attenuators and phase shifters have discrete values, thus, the quantization errors may not be avoided. Table 4 lists the optimized results based on the 3-D optimization target of the PWG with 8×8 elements by using the attenuators with a maximum range of 30 dB and minimum step of 0.5 dB, and 6-bit phase shifters with a minimum step of 5.625°. For comparison, those results with continued values shown in Table 2 are also listed in the second column of Table 4, from which we can see that both amplitude and phase distributions deteriorate when those excited continued values of source elements are quantized. The quantization errors may be reduced by two methods, one is named pre-optimization which uses the quantized discrete

TABLE 4. Optimization deviations based on different methods.

Field distribution	Deviations of amplitude (dB) /phase (°)			
	continue	quantization	pre-opt.	post-opt.
X-axis	0.89/5.42	1.03/ 6.96	1.03/ 6.23	0.87/ 8.65
XOY plane	1.02/14.85	1.18/15.90	1.11/15.95	1.01/14.74
XOZ plane	0.69/11.01	1.05/12.00	1.03/ 8.70	0.87/12.28
YOZ plane	1.02/14.85	1.18/15.90	1.11/15.95	1.01/14.74
3-D sphere	1.09/14.89	1.34/16.83	1.13/15.95	1.12/15.14

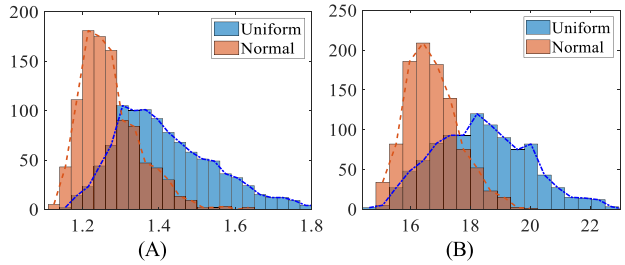

FIGURE 20. The statistical characteristics of the (A) amplitude and (B) phase with the distributions of uniform and normal errors.

values rather than continued values during the optimization process, and the other one is named post-optimization, which is to re-run the quantized optimization based on the initial values obtained from the first optimization using continued excitations. The optimized results using pre-optimization and post-optimization are also listed in Table 4, we can see that both pre- and post-optimization help to improve the optimized results from quantization values with few gaps remaining to the results from continuing excitations.

Furthermore, random errors from the attenuators and phase shifters are unavoidable as well, Figure 20 shows the statistical results by using the Monte Carlo method [33] based on amplitude and phase errors of ± 0.25 dB and $\pm 2.5°$ with uniform and normal distributions. Compared to the post-optimized results in the 3-D sphere listed in Table 4, it is obvious that those random errors deteriorate the field distributions of QZ further. This problem may be solved by recoding the errors of attenuators and phase shifters at each frequency point in advance and then running the optimization process considering these coherent factors.

C. FURTHER CONSIDERATION

The traditional local optimal solution requires a correct initial value to synthesize the excitations of the source element; however, the solution space is potentially to be very huge when the count of the source element increases and the synthesis process could be taken as a non-convex optimization, this will cause the problem to find the true solution. In this work, the LSM obtains the initial possible solution which is used as the starting point of the GA. This solution may be ill-conditioned; however, it may be close to the effective solution and can be used for the GA jumping out of the local

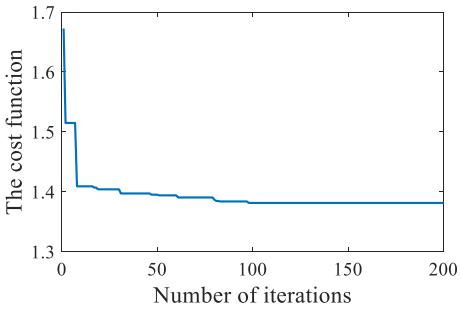

FIGURE 21. The cost function convergence of GA based on the initial value from LSM.

optimal solution. This is the reason that the hybrid algorithm has higher efficiency than that of the GA starting from the initial state.

The optimizations in this work mainly run on a laptop with a CPU of AMD Ryzen^{TM} 5 5500U and 16 G memory, those key parameters such as the crossover probability, the mutation probability, and the population number are 0.7, 0.3, and 50. The numbers of optimized field points are 10000 and 25000, and the calculation times are approximately 30 seconds and 15 minutes based on the 2-D and 3-D optimization of the source array with 8×8 elements, respectively. Figure 21 shows the convergence rate of the hybrid algorithm in which the cost function converges from 1.65 to 1.4 in the first 30 iterations and then converges to 1.38 in the left 170 iterations based on the 3-D optimization of the source array with 8×8 elements. However, when the source array has 32×32 elements the maximum calculation time is up to 10 minutes and 2.5 hours in 2-D and 3-D optimization when the maximum iteration is 200, respectively. Detailed information on the GA cost function is available in Section IV-B.

Furthermore, we propose a synthesis method in the entire full 3D-spherical to improve the performances of the QZ and the hybridizing technology of LSM and GA with high efficiency based on the ideal model. However, it could be a criterion of the antenna measurement and guidance of the PWG design, along with the recommended consideration of QZ 3D spherical region.

In the real experiment, many things such as the performances of the actual probe, the polarization, the environment, and the mutual couplings cannot be avoided and need to be involved in the consideration of actual antenna array during the synthesis. Meanwhile, a wide band antenna in PWG will be used and its amplitudes/phases will be synthesized at each frequency point to ensure the measurement accuracy for wide spectrum measurements.

VII. CONCLUSION

We propose a hybrid method with LSM and GA to synthesize the amplitude and phase weights of source elements in the PWG for the creation of a 3-D sphere QZ. After briefly describing the measurement system, the synthesis model, and the basic concepts of LSM and GA, the approach, process,

and key factors of the proposed concept are demonstrated in detail. The synthesis of PWGs with an 8-element linear array and the 8 × 8-element plane array is performed, the results are compared with several existing arts, and errors are discussed. It shows that our approach can create a more robust and better field distribution in a targeted 3D region than the traditional regression approaches do.

REFERENCES

[1] R. Wang, X. Wu, Y. Yang, S. Zhu, X. Zhao, and Z. Liu, "5G OTA testing: Challenges and standardization progress," in *Proc. IEEE Asia–Pacific Conf. Antennas Propag. (APCAP)*, 2018, pp. 469–470.

[2] F. Scattone et al., "Preliminary assessment of millimeter wave plane wave generator for 5G device testing," in *Proc. 15th Eur. Conf. Antennas Propag. (EuCAP)*, 2021, pp. 1–5.

[3] W. Fan, P. Kyosti, M. Rumney, X. Chen, and G. F. Pedersen, "Over-the-air radiated testing of millimeter-wave beam-steerable devices in a cost-effective measurement setup," *IEEE Commun. Mag.*, vol. 56, no. 7, pp. 64–71, Jul. 2018.

[4] S. Catteau, M. Ivashina, and R. Rehammar, "Design and simulation of a 28 GHz plane wave generator for NR measurements," in *Proc. 14th Eur. Conf. Antennas Propag. (EuCAP)*, 2020, pp. 1–4.

[5] K. Per-Simon, *Foundations of Antenna Engineering: A Unified Approach for Line-of-Sight and Multipath*. Boston, MA, USA: Artech, 2015.

[6] F. Scattone et al., "Towards testing of 5G millimeter wave devices using plane wave generators," in *Proc. 15th Eur. Conf. Antennas Propag. (EuCAP)*, 2021, pp. 1–4.

[7] J. Wang, Z. Yan, C. Fu, Z. Ma, and J. Liu, "Near-field precision measurement system of high-density integrated module," *IEEE Trans. Instrum. Meas.*, vol. 70, pp. 1–9, May 2021, doi: 10.1109/TIM.2021.3078000.

[8] H. Chen and T. K. Sarkar, "Using Planar probe array near field measurement to obtain accurate far field antenna pattern efficiently," in *Proc. IEEE Int. Conf. Computat. Electromagn. (ICCEM)*, 2019, pp. 1–3.

[9] A. Yaghjian, "An overview of near-field antenna measurements," *IEEE Trans. Antennas Propag.*, vol. 34, no. 1, pp. 30–45, Jan. 1986.

[10] *IEEE Standard Test Procedures for Antennas*, ANSI/IEEE Standard 149-1979, 1979.

[11] R. Haupt, "Synthesis of a plane wave in the near field with a planar phased array," in *Proc. IEEE Antennas Propag. Soc. Int. Symp. Dig. USNC/CNC/URSI North Amer. Radio Sci. Meeting*, 2003, pp. 792–795.

[12] A. Capozzoli, C. Curcio, G. D. Elia, A. Liseno, and P. Vinetti, "A novel approach to the design of generalized plane-wave synthesizers," in *Proc. 3rd Eur. Conf. Antennas Propag.*, 2009, pp. 3375–3379.

[13] "Technical specification group radio access network; radio frequency (RF) conformance testing background for radiated base station (BS) requirements," 3GPP, Sophia Antipolis, France, Rep. TR 37.941 V17.1.0, Jun. 2023.

[14] O. M. Bucci, M. D. Migliore, G. Panariello, and D. Pinchera, "Plane-wave generators: Design guidelines, achievable performances and effective synthesis," *IEEE Trans. Antennas Propag.*, vol. 61, no. 4, pp. 2005–2018, Apr. 2013.

[15] D. A. Hill, "A numerical method for near-field array synthesis," *IEEE Trans. Electromagn. Compat.*, vol. EMC-27, no. 4, pp. 201–211, Nov. 1985.

[16] S. Sun, N. Wang, X. Ma, S. Zhu, and R. Wang, "Design of plane wave generator in compact range for 5G OTA testing," in *Proc. Photon. Electromagn. Res. Symp. (PIERS)*, 2019, pp. 1011–1014.

[17] F. Peng, X. Chen, H. Pei, M. Zhang, J. Zhang, and Z. Ji, "Investigation of array-based plane wave generator for compact antenna test range application," in *Proc. Int. Conf. Microw. Millimeter Wave Technol. (ICMMT)*, 2020, pp. 1–3.

[18] P. S. Krasov, O. A. Iupikov, R. Maaskant, A. A. Glazunov, R. Rehammar, and M. V. Ivashina, "Quiet zone quality of a plane wave generator inside an over-moded waveguide chamber emulating a variable angle of incidence," in *Proc. 15th Eur. Conf. Antennas Propag. (EuCAP)*, 2021, pp. 1–5.

[19] O. M. Bucci, M. D. Migliore, G. Panariello, and D. Pinchera, "Plane-wave generators: Design guidelines, achievable performances and effective synthesis," *IEEE Trans. Antennas Propag.*, vol. 61, no. 4, pp. 2005–2018, Apr. 2013.

[20] O. M. Bucci, M. D. Migliore, G. Panariello, and D. Pinchera, "An effective algorithm for the synthesis of a plane wave generator for linear array testing," in *Proc. IEEE Int. Symp. Antennas Propag.*, 2012, pp. 1–2.

[21] S. Zhu, Z. Wang, Y. Zhang, and J. Miao, "Wideband plane wave generator with fixed amplitude excitation at sub-6GHz," in *Proc. IEEE Conf. Antenna Meas. Appl. (CAMA)*, 2021, pp. 353–356.

[22] X. Sun, Z. Wang, and J. Miao, "Near field quasi plane wave generation and performance evaluation," in *Proc. Asia–Pacific Microw. Conf. (APMC)*, 2018, pp. 917–919.

[23] F. Scattone et al., "Design of dual polarised wide band plane wave generator for direct far-field testing," in *Proc. 13th Eur. Conf. Antennas Propag. (EuCAP)*, 2019, pp. 1–4.

[24] V. M. Jayakrishnan and M. L. Liya, "A survey on automatic antenna rotator system," in *Proc. 5th Int. Conf. I-SMAC (IoT in Social, Mobile, Anal. Cloud) (I-SMAC)*, 2021, pp. 1659–1662.

[25] *IEEE Recommended Practice for Antenna Measurements*, IEEE Standard 149-2021 (Revision of IEEE Std 149-1977), 2022.

[26] J. H. Ginsberg, "Spherical waves and point sources," in *Acoustics-A Textbook for Engineers and Physicists: Volume I: Fundamentals*. Cham, Switzerland: Springer, 2018, pp. 433–567.

[27] C. Xudong, "Least Squares," in *Computational Methods for Electromagnetic Inverse Scattering*. Singapore: Wiley, 2018, pp. 291–294.

[28] K. Choi, D.-H. Jang, S.-I. Kang, J.-H. Lee, T.-K. Chung, and H.-S. Kim, "Hybrid algorithm combing genetic algorithm with evolution strategy for antenna design," *IEEE Trans. Magn.*, vol. 52, no. 3, pp. 1–4, Mar. 2016.

[29] X. Lin, S. Ke, Z. Li, H. Weng, and X. Han, "A fault diagnosis method of power systems based on improved objective function and genetic algorithm-tabu search," *IEEE Trans. Power Del.*, vol. 25, no. 3, pp. 1268–1274, Jul. 2010.

[30] R. S. Xie et al., "Synthesis of plane wave applied to 5G communication antenna measurement," in *Proc. Progress Electromagn. Res. Symp. Spring (PIERS)*, 2017, pp. 195–198.

[31] Z. Yang, Z. Wang, Y. Zhang, and S. Gao, "Robust plane wave generator design in small anechoic chamber setup using parameterized field method," *IEEE Access*, vol. 8, pp. 187052–187059, 2020.

[32] H. Wang et al., "Effective sparse recovery framework for ultrawideband robust plane wave generator," *IEEE Antennas Wireless Propag. Lett.*, vol. 22, no. 3, pp. 462–466, Mar. 2023.

[33] L. Jeongheum, L. Yongbeum, and K. Hyeongdong, "Decision of error tolerance in array element by the Monte Carlo method," *IEEE Trans. Antennas Propag.*, vol. 53, no. 4, pp. 1325–1331, Apr. 2005.

HAIDONG CHEN (Senior Member, IEEE) received the B.Sc., M.Sc., and Ph.D. degrees from the Nanjing University of Science and Technology (NUST), Nanjing, China, in 2001, 2009, and 2017, respectively.

In 2001, he was with the 14th Research Institute, CETC, Nanjing. In 2008, he was with Andrew Telecommunication, Suzhou, China. From 2014 to 2016, he was a Research Assistant with the University of Michigan at Ann Arbor, Ann Arbor, MI, USA. From 2017 to 2019, he was a Lecturer with NUST. In 2017, he joined the South China University of Technology, Guangzhou, China, where he is currently an Associate Professor with the School of Electronics and Information Engineering. His current research interests include microwave/millimeter-wave circuits, measurements, and new materials applications.

WEIJUN ZHONG received the B.Sc. degree from the Nanjing University of Posts and Telecommunications, Nanjing, China, in 2020, and the M.Sc. degree from the South China University of Technology, Guangzhou, China, in 2023. Her current research interests are the measurement of microwave and millimeter-wave antennas based on the plane-wave generator method.

MU TAN received the B.E. degree from the College of Information Science and Technology, Donghua University, Shanghai, China, in 2022. She is currently pursuing the M.S. degree in electromagnetic fields and microwave technology with the South China University of Technology, Guangzhou, China. Her current research interest is the synthesis of plane wave for measurement of microwave and millimeter-wave antennas.

ZHAOLING HE received the B.Sc. degree from Nantong University, Nantong, China, in 2020, and the M.Sc. degree from the South China University of Technology, Guangzhou, China, in June 2023.

In July 2023, he joined Huawei, Dongguan, and worked on the development of wireless. His current research interests are in RF and OTA measurement for mobile communication devices.

TING LI received the B.E. degree in Internet of Things engineering from Hunan Normal University, Changsha, China, in 2021. She is currently pursuing the M.S. degree in electromagnetic fields and microwave technology with the South China University of Technology, Guangzhou, China. Her current research interests are the key algorithms for near-field measurement of microwave and millimeter-wave antennas.

QUAN XUE (Fellow, IEEE) received the B.S., M.S., and Ph.D. degrees in electronic engineering from the University of Electronic Science and Technology of China (UESTC), Chengdu, China, in 1988, 1991, and 1993, respectively.

In 1993, he joined UESTC, as a Lecturer, where he became a Professor in 1997. From October 1997 to October 1998, he was a Research Associate and then a Research Fellow with The Chinese University of Hong Kong, Hong Kong. In 1999, he joined the City University of Hong Kong, Hong Kong, where he was a Chair Professor of Microwave Engineering, and served as an Associate Vice President (Innovation Advancement and China Office) from June 2011 to January 2015, the Director of the Information and Communication Technology Center, and the Deputy Director of the State Key Laboratory of Millimeter Waves, Hong Kong. In 2017, he joined the South China University of Technology, Guangzhou, China, where he is currently a Professor and the Dean of the School of Electronics and Information Engineering and the Director of the Guangdong Provincial Key Laboratory of Millimeter-Wave and Terahertz. He has authored or coauthored more than 400 internationally refereed journal articles and more than 160 international conference papers. He is also a coinventor of five granted Chinese patents and 15 granted U.S. patents, in addition to 26 filed patents. His research interests include microwave/millimeter-wave/terahertz passive components, active components, antenna, microwave monolithic integrated circuits, and radio frequency integrated circuits.

Prof. Xue was a recipient of the 2017 H. A. Wheeler Applications Prize Paper Award. He has served as an Associate Editor for the IEEE TRANSACTIONS ON MICROWAVE THEORY AND TECHNIQUES from 2010 to 2013 and the IEEE TRANSACTIONS ON INDUSTRIAL ELECTRONICS from 2010 to 2015, and an Editor for the *International Journal of Antennas and Propagation* from 2010 to 2013. He was an Associate Editor of the IEEE TRANSACTIONS ON ANTENNAS AND PROPAGATION. He has served as an AdCom Member of the IEEE MTT-S from 2011 to 2013.

WENQUAN CHE (Fellow, IEEE) received the B.Sc. degree from the East China Institute of Science and Technology, Nanjing, China, in 1990, the M.Sc. degree from the Nanjing University of Science and Technology (NUST), Nanjing, in 1995, and the Ph.D. degree from the City University of Hong Kong, Hong Kong, in 2003.

In 1999, she was a Research Assistant with the City University of Hong Kong. In 2002, she was a Visiting Scholar with the Polytechnique de Montreal, Montreal, QC, Canada. From 2007 to 2008, she conducted academic research with the Institute of High-Frequency Technology, Technische Universität München, Munich, Germany. From 2005 to 2006 and from 2009 to 2012, she was with the City University of Hong Kong as a Research Fellow and a Visiting Professor, respectively. She was a Professor with NUST, from 2008 to 2018. She joined the South China University of Technology, Guangzhou, China, as a Professor, in November 2018. She has authored or coauthored over 300 internationally refereed journal articles and more than 120 international conference papers. Her current research interests include microwave and millimeter-wave circuits and systems, microwave monolithic integrated circuits, antenna technologies, and the medical applications of microwave technologies.

Dr. Che was a recipient of the 2007 Humboldt Research Fellowship presented by the Alexander von Humboldt Foundation of Germany, the 5th China Young Female Scientists Award in 2008, and the Distinguished Young Scientist Award by the National Natural Science Foundation Committee of China in 2012. She has been a Reviewer of the *IET Microwaves, Antennas and Propagation*. She is also a Reviewer of the IEEE TRANSACTIONS ON MICROWAVE THEORY AND TECHNIQUES, the IEEE TRANSACTIONS ON ANTENNAS AND PROPAGATION, the IEEE TRANSACTIONS ON INDUSTRIAL ELECTRONICS, and the IEEE MICROWAVE AND WIRELESS COMPONENTS LETTERS. She is the Editor-in-Chief of the *Microwave and Optical Technology Letters*. She is an Elected Member of the IEEE MTT-S AdCom.